Available online at sjuoz.uoz.edu.krd

Science Journal of University of Zakho

Vol. 8, No. 1, pp. 23– 28, March-2020

p-ISSN: 2663-628X
e-ISSN: 2663-6298

STRUCTURAL, ELECTRONIC AND OPTICAL PROPERTIES OF CUBIC PEROVSKITE $CsPbX_3$ (X= Br, Cl and I)

Nawzad A. Abdulkareem [a,*], Sarkawt A. Sami [b], Badal H. Elias [b]

[a] Dept. of Physics, Faculty of Science, University of Zakho, Kurdistan Region-Iraq - (nawzad.abdulkareem@uoz.edu.krd)
[b] Dept. of Physics, College of Science, University of Duhok, Kurdistan Region - Iraq - (sarkawt@uod.ac; bader_hyder@yahoo.com)

Received: Aug., 2019 / Accepted: Nov., 2019 / Published: Mar.,2020 ***https://doi.org/10.25271/sjuoz.2020.8.1.632***

ABSTRACT:
Plane waves with norm conserving pseudopotentials (PW-PP) method in conjunction with density functional theory (DFT) frame work have been used to investigate structural, electronic and optical properties of lead-halide cubic perovskite CsPbX3 (X=Br, Cl and I). The generalized gradient approximation (GGA), specifically Perdew-Burke-Ernzerhof (PBE) flavor, has been chosen to treat the exchange correlation term of Kohn-Sham equation. Structural parameters are comparable with other theoretical and experimental studies. In spite of good agreement of our band gap values E_g with other theoretical works, however, they were not comparable when compared to the experimental E_g values due to the well-known problem of E_g value underestimation of DFT. To update the E_g value, we have used GW method as a self-consistent quasiparticle method on energies and wave functions and indeed they have been improved. Optical properties have been calculated using density functional perturbation theory (DFPT). Our results show that $CsPbX_3$ (X=Br, Cl, I) has maximum response to the electromagnetic spectrum at low energies (visible region) but minimum response at high energies.

KEYWORDS: Ab initio calculation; Structural, electrical and optical properties; Band gap; Perovskites $CsPbX_3$.

1. INTRODUCTION

Perovskite-based compounds (with formula ABX3) have been studied intensively in the recent years as promising materials for light emitting diodes (LED)(Song et al., 2015; Tan et al., 2014), photodetectors (Dong et al., 2015; Wei et al., 2016) and for low-cost solar cells with relatively high efficiency, up to 22.1%(Kim et al., 2012; Kojima, Teshima, Shirai, & Miyasaka, 2009; Y. Li, Duan, Zhao, & Tang, 2018; Mutalikdesai & Ramasesha, 2017; Zhou et al., 2014), because of their good electronic and optical properties. However, potential stability is the most challenge which hamper mass production of perovskite-based solar cells (Z. Li et al., 2015). Organometallic halide perovskite (OHP) (where A is organic cation, B is metal cation and X is halide anion) and inorganic halide perovskite (IHP) (for example, A=Cs) have been studied. In spite of instability of both groups, the latter group is more promising because the OHP are highly sensitive to moisture and other ambient environment conditions (X. Li et al., 2017). Among IHP, $CsPbX_3$ (X=Br, Cl and I) are direct and tunable band gap semiconductors (Castelli, García-Lastra, Thygesen, & Jacobsen, 2014). The three compounds show phase transition, $CsPbBr_3$ has orthorhombic structure at room temperature and undergoes phase transition to tetragonal at 88 [°C] and to the cubic at 130 [°C] (MØLLER, 1958; Stoumpos et al., 2013), $CsPbCl_3$ undergoes phase transition from tetragonal structure or monoclinic to cubic perovskite at 47 °C (MØLLER, 1958) and $CsPbI_3$, which is orthorhombic, becomes perovskite cubic above 316 °C (Surendra Sharma, Weiden, & Weiss, 1992).
The $CsPbBr_3$ meets sufficient requirements for photoelectronic devices such as x-ray and γ-ray detectors (Stoumpos et al., 2013) and long-term stability solar cells with efficiencies 6.95% and 5.37 % (Lei et al., 2018). A cubic perovskite $CsPbI_3$ solar cell has been fabricated with efficiency up to 2.9% with fair stability at room temperature (Eperon et al., 2015).
A number of theoretical works on $CsPbX_3$ (X=Br, Cl and I) have been published. Lang et al (Lang, Yang, Liu, Xiang, & Gong, 2014) calculated imaginary part of dielectric function and electronic band structure implementing the projector augmented-wave (PAW) pseudopotentials (Kresse & Joubert, 1999) in the framework of density functional theory (DFT) using the Vienna ab-initio simulation package (VASP) (Kresse & Furthmüller, 1996). Chang and Park (Chang, Park, & Matsuishi, 2004) investigated structural and electronic properties of $CsPbX_3$ theoretically using first-principles pseudopotential total-energy calculations within the local density approximation (LDA). All electrons full potential linearized augmented plane wave (FP–LAPW) method was implemented to calculate structural, electronic, and optical properties of cubic perovskites $CsPbX_3$ using the wien2k code (Murtaza & Ahmad, 2011). Structural, electronic and optical properties of three compounds CsPbX3 have been calculated using full potential linearized augmented plane waves method within DFT and for accurate band gap values, modified Becke-Johnson (TB-mBJ) exchange potential has been employed (Ahmad et al., 2017).
The aim of this study is to investigate structural, electronic and optical properties using DFT frame. The augmented plane waves (PW) with norm-conserving, separable, dual-space Gaussian-type pseudopotentials of Goedecker, Teter and Hutter scheme (GTH) (Hartwigsen, Gœdecker, & Hutter, 1998) with generalized gradient approximation (GGA) of DFT (Perdew, Burke, & Ernzerhof, 1996) have been used to calculate structural, electric and optical properties of the perovskites $CsPbX_3$ (X=Br, Cl, I). Perdew-Burke- Ernzerhof (PBE) has been chosen to treat

* Corresponding author

exchange-correlation term of DFT Kohn-Sham total energy equation (Kohn & Sham, 1965). To obtain accurate value of the fundamental band gap, we have used GW approximation (Hedin, 1965).

2. COMPUTATIONAL METHOD

In the present work, DFT framework in conjunction with PW and norm-conserving pseudopotentials has been used to calculate structural, electronic and optical properties of $CsPbX_3$ (X=Br, Cl and I). The GTH separable, dual-space Gaussian-type pseudopotentials (Krack, 2005) have been employed as it treats $5s^2\ 5p^6\ 6s^1$ of Cs, $5d^{10}\ 6s^2\ 6p^2$ of Pb, $4s^2\ 4p^5$ of Br, $3s^2\ 3p^5$ of Cl and $5s^2\ 5p^5$ of I as valence states. Our calculations have been done using Abinit package (Gonze et al., 2009).

Cubic perovskite structure (ABX_3) has 5 atoms per unit cell. The five atoms taken into account are located as follows: A at 0.0 0.0 0.0, B at 0.5 0.5 0.5 and X_3 atoms occupy 0.5 0.5 0.0, 0.5 0.0 0.5 and 0.0 0.5 0.5 (figure 1).

First, convergence calculations have been done to result in the cut-off energy of 1088 [eV] and the number of k points of 40 points, which corresponds to the Monkhorst–Pack (Monkhorst & Pack, 1976) k-point mesh of 6×6×6. Then we have optimized lattice constant a and atomic coordinates using GGA-PBE method. The optimized a and relaxed atomic coordinates were employed to compute band structure and band gap values E_g. Moreover, total density of states (TDOS) and partial density of states (PDOS) have been computed. Due to the familiar underestimation of band gap problem of DFT (Perdew, 1986), GW method (Hedin, 1965) as a self-consistent quasiparticle method on energies and wavefunctions was used to update and to get E_g values comparable with experimental results. Optical properties have been calculated using density functional perturbation theory (DFPT) (S Sharma & Ambrosch-Draxl, 2004) and Kramers-Kronig relations (Collins et al., 2001).

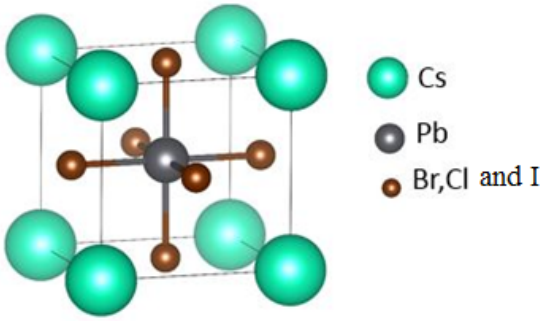

Figure 1. The cubic structure of $CsPbX_3$ perovskite

3. RESULTS AND DISCUSSION

3.1 Structural properties

Optimization was done for (a) and atomic coordinates of the three compounds. Employing the relaxed atomic coordinates, the total energy (E_T) and pressure were calculated for various values of (a). Figure 2 shows the E_T plots against a, from which the optimized a values for the three compounds were taken, and figure 3 displays the change of pressure with the volume of the unit cell.

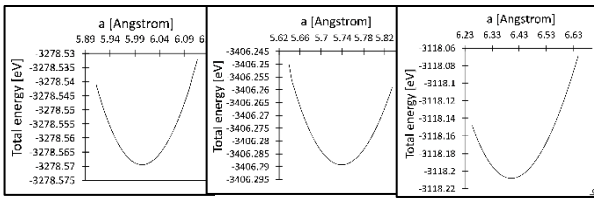

Figure 2. Total energy versus lattice parameter of (a) $CsPbBr_3$ (b) $CsPbCl_3$ and (c) $CsPbI_3$

Figure 2. Total energy versus lattice parameter of (a) $CsPbBr_3$ (b) $CsPbCl_3$ and (c) $CsPbI_3$

The change of pressure P with the volume V of the unit cell for each compound, see figure 3, was fitted to the second-order Birch-Murnaghan equation of state (Birch, 1947; Murnaghan, 1944):

$$P(V) = \frac{3B_o}{2}\left[\left(\frac{V_o}{V}\right)^{7/3} - \left(\frac{V_o}{V}\right)^{5/3}\right]\left[1 + \frac{3}{4}\left(B_o' - 4\right)\left\{\left(\frac{V_o}{V}\right)^{2/3} - 1\right\}\right] \quad (1)$$

Where V_o is the cell volume at zero pressure, B_o is the bulk modulus and B_o' is the derivative of bulk modulus with respect to pressure. From the fittings, we obtained the values of B_o of the three compounds and they are given in Table 1 along with their V_o values. The optimized structural properties, calculated in GGA-PBE, as well as results of other work are also displayed in Table 1.

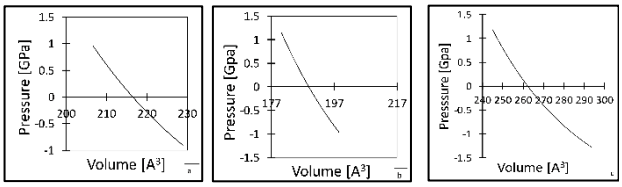

Figure 3. Pressure evolution of unit cell volume of (a) $CsPbBr_3$, (b) $CsPbCl_3$ and (c) $CsPbI_3$.

Table 1. Optimized structural properties calculated in GGA-PBE compared with experimental and other theoretical results

	$CsPbBr_3$			$CsPbCl_3$			$CsPbI_3$		
Parameter	Present work	Exp.	Other theoretical works	Present work	Exp.	Other theoretical works	Present work	Exp.	Other theoretical works
a [Angstrom]	6.007	5.87[a]	6.046[b]	5.738	5.6[a]	5.783[b]	6.397	6.289[c]	6.461[b]
E_T [eV]	-3278.56			-3406.28			-3118.2		
B_o [GPa]	18.06		18.1[d]	22.09		22.59[e]	13.02		19.8[f]
V_o [A^3]	216.756			189.012			261.77		
Bonds length [Angstrom]									
Cs-Br	4.245		4.15[g]						
Pb-Br	3.002		2.935[g]						
Cs-Cl				4.0578		6.883[g]			
Pb-Cl				2.8693		2.810[g]			
Cs-I							4.526		4.137[g]
Pb-I							3.2		5.406[g]

a ref.(MØLLER, 1958), b ref. (Ye et al., 2015), c ref. (Trots & Myagkota, 2008), d ref (Zhang, Zeng, & Wang, 2017), e ref. (Hu, Ge, Yu, & Feng, 2017), f ref. (Murtaza & Ahmad, 2011), g ref. (Ahmad et al., 2017).

There is, mostly, good agreement of our results with experimental results and with other theoretical works, which have been done using different implementations of DFT. Lattice parameter values of $CsPbBr_3$, $CsPbCl_3$ and $CsPbI_3$ are in error with experimental values by 2.3%, 2.4% and 1.7%, respectively. The Bulk modulus values of $CsPbBr_3$, $CsPbCl_3$ have errors of 0.16% and 2.19%, respectively, while that of $CsPbI_3$ has an error of 34.24%. The bond lengths are also in very good agreement except for Cs-Cl bond of $CsPbCl_3$ and Pb-I bond of $CsPbI_3$.

3.2 Electronic properties

Electronic shape and nature are described by electronic band structure and density of states (DOS), and both have been computed using GGA-PBE method. Figure 4 shows band structure of $CsPbBr_3$, $CsPbCl_3$ and $CsPbI_3$ compounds. The band structures shown in figure 4 confirm that the three compounds are semiconductors. The little difference in the band structure shape of the three compounds is attributed to the difference of halogen atom (Br, Cl and I)

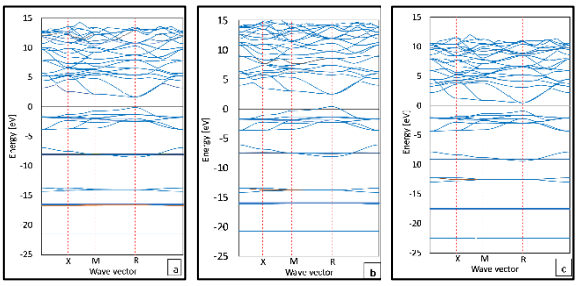

Figure 4. Band structure of (a) $CsPbBr_3$, (b) $CsPbCl_3$ and (c) $CsPbI_3$. The PED-GGA method of DFT was used.

It is confirmed that the cesium based lead-halide perovskites have a direct fundamental band gap E_g between bands 22 and 23. Minimum of the conduction band (CBM) and maximum of the valence band (VBM) both are located at the symmetry point R. Notably, bands 23, 24 and 25 are degenerate, that is, more states for electron transition from VB; this makes these compounds even more significant. Band gap values at high symmetry points including the fundamental band gap are listed in table 2.

Table 2. Calculated energy gaps (in [eV]) at some high symmetry points in PBE-GGA method. Results of other theoretical and experimental works are also given.

	$E^{\Gamma-\Gamma}$	E^{X-X}	E^{M-M}	E^{R-R}
$CsPbBr_3$ Present work Theoretical work Experiment	 4.91 5.05[a]	 3.85 4.5[a]	 2.82 3.05[a]	 1.75 1.6[a] 2.3[c]
$CsPbCl_3$ Present work Theoretical work Experiment	 5.69 5.5[a]	 4.52 4.6[a]	 3.37 3.2[a]	 2.18 1.8[a] 3.0[c]
$CsPbI_3$ Present work Theoretical work Experiment	 4.21 4.2[a]	 3.04 3.6[a]	 2.29 2.4[a]	 1.46 1.3[a] 1.73[b]

a ref. (Murtaza & Ahmad, 2011), b ref. (Eperon et al., 2014), c ref. (Heidrich et al., 1981).

There is good agreement between our results in Table 2 and other theoretical results, except for the value of the fundamental band gap $E_g = E^{R-R}$, which does not agree with experimental data. This discrepancy is attributed to the underestimation of the PBE-GGA method of the fundamental band gap value, which is a well-known problem of DFT. GW method has been used to correct the value of E_g. Table 3 shows improvement of the calculated E_g values after implementing the GW method. Fundamental band gap values of $CsPbX_3$ (X=Br, Cl and I), calculated using PBE-GGA, are in error with experimental values by 25.49%, 27.16%

and 15.4%, respectively, but when we have used GW method, they have been improved, and the errors reduced to 2.54%, 6.66% and 10.8 %, respectively. It is clear from the fundamental band gap values that $CsPbCl_3$ has largest band gap which can be attributed to the smaller atomic number of Cl compared to those of Br and I atoms. Higher atom number means more number of protons that are electrostatically attracting and hence lowering the bonding energy and band gap as well.

Table 3. Fundamental band gap calculated using PBE-GGA and GW along with results of other theoretical and experimental works.

	$E_g = E^{R-R}$ [eV]		
	PBE-GGA	GW	Experimental
$CsPbBr_3$			
Present work	1.75	2.42	2.36[c]
Other works	1.61[a]	2.36[f]	
$CsPbCl_3$			
Present work	2.18	3.2	3[e]
Other works	2.16[a]	3.27[f]	
$CsPbI_3$			
Present work	1.46	1.91	1.73[d]
Other works	1.47[a], 1.3[b]	1.96[f]	

a ref. (Ahmad et al., 2017),b ref. (Murtaza & Ahmad, 2011), c ref. (Kulbak, Cahen, & Hodes, 2015), d ref. (Eperon et al., 2014), e ref. (Gesi, Ozawa, & Hirotsu, 1975), f ref. (Becker et al., 2018).

Total density of states (DOS) and partial density of states (PDOS) are more descriptive of the electronic nature of $CsPbX_3$ (X=Br, Cl and I) compounds. Figure 5 shows the calculated DOS and PDOS where the latter establishes the contribution of each atom to DOS. The DOS is plotted in the range of –20 to 20 [eV], however the states start to appear at about –17 [eV]. Fermi level in our calculations are located at –0.22 [eV], 0.2 [eV] and –1.11 [eV] for $CsPbBr_3$, $CsPbCl_3$ and $CsPbI_3$, respectively. The Fermi level energy values confirm that the compounds $CsPbX_3$ (X=Br, Cl and I) are semiconductors.

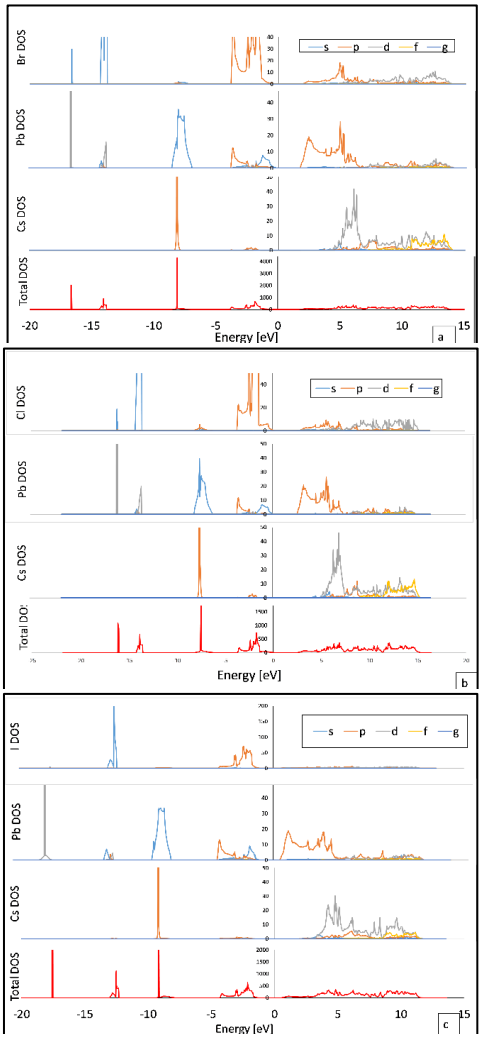

Figure 5. Total and partial DOS of (a) $CsPbBr_3$, (b) $CsPbCl_3$ and (c) $CsPbI_3$ calculated using PBE-GGA functional.

The PDOS describes the contributions of each atomic state to the DOS. For $CsPbX_3$ (X=Br, Cl and I), DOS at VB is mostly due to the contribution of the p state of the halogen atom (Br, Cl, and I), moreover, p state and s states of Pb are also involved. The CB are mostly due to the contributions of the d state of Cs and p state of Pb, see figure 5.

3-3 Optical properties

The $CsPbX_3$ (X=Br, Cl and I) are considered promising materials to future efficient solar cells from the point of view of their band gap values (Eperon et al., 2015; Lei et al., 2018; Stoumpos et al., 2013) and high optical response to the electromagnetic spectrum. We have calculated the frequency dependent linear optical properties, namely, imaginary part of dielectric function $\left(\mathrm{Im}(\varepsilon(\omega))\right)$, real part of dielectric function $(\mathrm{Re}(\varepsilon(\omega)))$, refractive index $n(\omega)$ and absorption coefficient $(\alpha(\omega))$. The results are shown in figure (6).

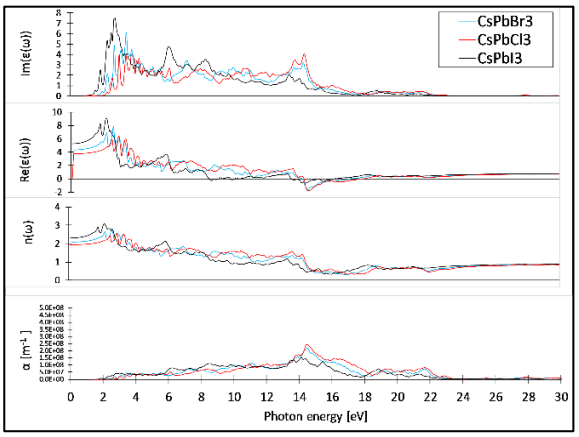

Figure 6. Optical properties of CsPbX3 (X=Br, Cl and I).

We have investigated optical properties response to the photon energies starting from 0 to 30 [eV] in steps of 0.0186 [eV]. The imaginary part of the dielectric function $\left(\mathrm{Im}(\varepsilon(\omega))\right)$ indicates absorption limits of the materials and energy gain ability as solar cells. The real part $\left(\mathrm{Re}(\varepsilon(\omega))\right)$ indicates energy store ability of the material. Let us divide the $\left(\mathrm{Im}(\varepsilon(\omega))\right)$ curve into two main regions: a low energy region and a high energy region, and discuss it in conjunction with band gap and DOS. In the low energy region, electron transitions occurs from p valence state of the halogen (Br, Cl and I) to the p conduction state of Pb, in this region $CsPbI_3$ has the highest peak due to its lowest band gap among these materials, therefore, it has maximum response to the visible light. At high energies, the response is due to the electron transitions from mixed s valence state of Pb and p valence state of Cs to the mixed p conduction state of Pb and d and p conduction states of Cs (Murtaza & Ahmad, 2011). In the high energy region, $CsPbCl_3$ has maximum peak followed by a lower peak for $CsPbBr_3$ then a lowest for $CsPbI_3$. This occurs because $CsPbCl_3$ has higher DOS in the p state of Pb in the VB which contains more electrons, thus leading to more transitions from VB to the CB. Similar trend of explanation can be used for the other optical properties. For example, maximum peak of absorption coefficient $\alpha(\omega)$ at visible light region (low energy) for $CsPbCl_3$, $CsPbBr_3$ and $CsPbI_3$ are 2.59×10^7, 2.62×10^7 and 4.45×10^7 $[m^{-1}]$, respectively. On the other hand, maximum peaks of $\alpha(\omega)$ in the high energy region are located at 2.42×10^8, 2.15×10^8 and 1.54×10^8 $[m^{-1}$]for $CsPbCl_3$, $CsPbBr_3$ and $CsPbI_3$, respectively .

From the real part of dielectric function $\left(\mathrm{Re}(\varepsilon(\omega))\right)$, the dielectric constant values can be found for any frequency. Its values at zero frequency $\varepsilon(0)$ are 3.69, 4.32 and 5.56 for $CsPbCl_3$, $CsPbBr_3$ and $CsPbI_3$, respectively. They increase with frequency and reach the maximum values at 2.93, 2.61 and 2.2 [eV], respectively, in the visible light region. Then, they decrease to negative value before they start again to increase slightly into less than one.

Refractive index $n(\omega)$ starts to increase until it reaches the maximum values of 2.54, 2.82 and 3.07 at energies 2.93, 2.61 and 2.2 [eV] for $CsPbCl_3$, $CsPbBr_3$ and $CsPbI_3$, respectively. $CsPbI_3$ has highest $n(\omega)$ which makes it a better material to retain energy than $CsPbBr_3$ and $CsPbCl_3$.

4. CONCLUSIONS

First principle calculations have been done here to investigate and review structural, electronic and optical properties of $CsPbX_3$ (X=Br, Cl and I). The structural properties have a good agreement with other theoretical works and experimental results. Moreover, it shows that $CsPbX_3$ (X=Br, Cl and I) have direct E_g between 22 and 23 bands located at the symmetry point R. The E_g values are comparable to the results obtained experimentally and theoretically using different implementations of DFT method by others.

The bands 23, 24 and 25 have the same energy (degenerate) thus accommodating more places for electrons to be excited from VB, hence leading to higher response to the electromagnetic excitation. Among $CsPbX_3$ (X=Br, Cl and I) group, $CsPbI_3$ has the highest response peak at visible light spectrum due to its E_g value. On the other hand, $CsPbCl_3$ has the highest response peak at high energy spectrum because it has a highest DOS specifically s state of Pb. The latter means more electrons available to transit to the CB.

REFERENCES

Ahmad, M., Rehman, G., Ali, L., Shafiq, M., Iqbal, R., Ahmad, R., . . . Ahmad, I. (2017). Structural, electronic and optical properties of CsPbX3 (X= Cl, Br, I) for energy storage and hybrid solar cell applications. *Journal of Alloys and Compounds, 705*, 828-839.

Becker, M. A., Vaxenburg, R., Nedelcu, G., Sercel, P. C., Shabaev, A., Mehl, M. J., . . . Lyons, J. L. (2018). Bright triplet excitons in caesium lead halide perovskites. *Nature, 553*(7687), 189.

Birch, F. (1947). Finite elastic strain of cubic crystals. *Physical review, 71*(11), 809.

Castelli, I. E., García-Lastra, J. M., Thygesen, K. S., & Jacobsen, K. W. (2014). Bandgap calculations and trends of organometal halide perovskites. *APL Materials, 2*(8), 081514.

Chang, Y., Park, C., & Matsuishi, K. (2004). First-principles study of the Structural and the electronic properties of the lead-Halide-based inorganic-organic perovskites (CH~ 3NH~ 3) PbX~ 3 and CsPbX~ 3 (X= Cl, Br, I). *Journal-Korean Physical Society, 44*, 889-893.

Collins, L., Bickham, S., Kress, J., Mazevet, S., Lenosky, T., Troullier, N., & Windl, W. (2001). Dynamical and optical properties of warm dense hydrogen. *Physical Review B, 63*(18), 184110.

Dong, Q., Fang, Y., Shao, Y., Mulligan, P., Qiu, J., Cao, L., & Huang, J. (2015). Electron-hole diffusion lengths> 175 μm in solution-grown CH3NH3PbI3 single crystals. *Science, 347*(6225), 967-970.

Eperon, G. E., Paterno, G. M., Sutton, R. J., Zampetti, A., Haghighirad, A. A., Cacialli, F., & Snaith, H. J. (2015). Inorganic caesium lead iodide perovskite solar cells. *Journal of Materials Chemistry A, 3*(39), 19688-19695.

Eperon, G. E., Stranks, S. D., Menelaou, C., Johnston, M. B., Herz, L. M., & Snaith, H. J. (2014). Formamidinium lead trihalide: a broadly tunable perovskite for efficient planar heterojunction solar cells. *Energy & Environmental Science, 7*(3), 982-988.

Gesi, K., Ozawa, K., & Hirotsu, S. (1975). Effect of hydrostatic pressure on the structural phase transitions in CsPbCl3 and CsPbBr3. *Journal of the Physical Society of Japan, 38*(2), 463-466.

Gonze, X., Amadon, B., Anglade, P.-M., Beuken, J.-M., Bottin, F., Boulanger, P., . . . Côté, M. (2009). ABINIT: First-principles approach to material and nanosystem properties. *Computer Physics Communications, 180*(12), 2582-2615.

Hartwigsen, C., Gœdecker, S., & Hutter, J. (1998). Relativistic separable dual-space Gaussian pseudopotentials from H to Rn. *Physical Review B, 58*(7), 3641.

Hedin, L. (1965). New method for calculating the one-particle Green's function with application to the electron-gas problem. *Physical Review, 139*(3A), A796.

Heidrich, K., Schäfer, W., Schreiber, M., Söchtig, J., Trendel, G., Treusch, J., . . . Stolz, H. (1981). Electronic structure, photoemission spectra, and vacuum-ultraviolet optical spectra of CsPb Cl 3 and CsPb Br 3. *Physical Review B, 24*(10), 5642.

Hu, M., Ge, C., Yu, J., & Feng, J. (2017). Mechanical and optical properties of Cs4BX6 (B= Pb, Sn; X= Cl, Br, I) zero-dimension perovskites. *The Journal of Physical Chemistry C, 121*(48), 27053-27058.

Kim, H.-S., Lee, C.-R., Im, J.-H., Lee, K.-B., Moehl, T., Marchioro, A., . . . Moser, J. E. (2012). Lead iodide perovskite sensitized all-solid-state submicron thin film mesoscopic solar cell with efficiency exceeding 9%. *Scientific reports, 2*, 591.

Kohn, W., & Sham, L. (1965). doi: 10.1103/PhysRev. 140. A1133. *Phys. Rev. A, 140*, 113.

Kojima, A., Teshima, K., Shirai, Y., & Miyasaka, T. (2009). Organometal halide perovskites as visible-light sensitizers for photovoltaic cells. *Journal of the American Chemical Society, 131*(17), 6050-6051.

Krack, M. (2005). Pseudopotentials for H to Kr optimized for gradient-corrected exchange-correlation functionals. *Theoretical Chemistry Accounts, 114*(1-3), 145-152.

Kresse, G., & Furthmüller, J. (1996). Efficiency of ab-initio total energy calculations for metals and semiconductors using a plane-wave basis set. *Computational materials science, 6*(1), 15-50.

Kresse, G., & Joubert, D. (1999). From ultrasoft pseudopotentials to the projector augmented-wave method. *Physical Review B, 59*(3), 1758.

Kulbak, M., Cahen, D., & Hodes, G. (2015). How important is the organic part of lead halide perovskite photovoltaic cells? Efficient CsPbBr3 cells. *The journal of physical chemistry letters, 6*(13), 2452-2456.

Lang, L., Yang, J.-H., Liu, H.-R., Xiang, H., & Gong, X. (2014). First-principles study on the electronic and optical properties of cubic ABX3 halide perovskites. *Physics Letters A, 378*(3), 290-293.

Lei, J., Gao, F., Wang, H., Li, J., Jiang, J., Wu, X., . . . Liu, S. F. (2018). Efficient planar CsPbBr3 perovskite solar cells by dual-source vacuum evaporation. *Solar Energy Materials and Solar Cells, 187*, 1-8.

Li, X., Cao, F., Yu, D., Chen, J., Sun, Z., Shen, Y., . . . Wu, Y. (2017). All inorganic halide perovskites nanosystem: synthesis, structural features, optical properties and optoelectronic applications. *Small, 13*(9), 1603996.

Li, Y., Duan, J., Zhao, Y., & Tang, Q. (2018). All-inorganic bifacial CsPbBr 3 perovskite solar cells with a 98.5%-bifacial factor. *Chemical communications, 54*(59), 8237-8240.

Li, Z., Yang, M., Park, J.-S., Wei, S.-H., Berry, J. J., & Zhu, K. (2015). Stabilizing perovskite structures by tuning tolerance factor: formation of formamidinium and cesium lead iodide solid-state alloys. *Chemistry of Materials, 28*(1), 284-292.

MØLLER, C. K. (1958). Crystal structure and photoconductivity of caesium plumbohalides. *Nature, 182*(4647), 1436.

Monkhorst, H. J., & Pack, J. D. (1976). Special points for Brillouin-zone integrations. *Physical Review B, 13*(12), 5188.

Murnaghan, F. (1944). The compressibility of media under extreme pressures. *Proceedings of the national academy of sciences of the United States of America, 30*(9), 244.

Murtaza, G., & Ahmad, I. (2011). First principle study of the structural and optoelectronic properties of cubic perovskites CsPbM3 (M= Cl, Br, I). *Physica B: Condensed Matter, 406*(17), 3222-3229.

Mutalikdesai, A., & Ramasesha, S. K. (2017). Emerging solar technologies: Perovskite solar cell. *Resonance, 22*(11), 1061-1083.

Perdew, J. P. (1986). Density functional theory and the band gap problem. *International Journal of Quantum Chemistry, 30*(3), 451-451.

Perdew, J. P., Burke, K., & Ernzerhof, M. (1996). Generalized gradient approximation made simple. *Physical review letters, 77*(18), 3865.

Sharma, S., & Ambrosch-Draxl, C. (2004). Second-harmonic optical response from first principles. *Physica Scripta, 2004*(T109), 128.

Sharma, S., Weiden, N., & Weiss, A. (1992). Phase diagrams of quasibinary systems of the type: ABX3—A′ BX3; ABX3—AB′ X3, and ABX3—ABX′ 3; X= halogen. *Zeitschrift für Physikalische Chemie, 175*(1), 63-80.

Song, J., Li, J., Li, X., Xu, L., Dong, Y., & Zeng, H. (2015). Quantum dot light-emitting diodes based on inorganic perovskite cesium lead halides (CsPbX3). *Advanced materials, 27*(44), 7162-7167.

Stoumpos, C. C., Malliakas, C. D., Peters, J. A., Liu, Z., Sebastian, M., Im, J., . . . Freeman, A. J. (2013). Crystal growth of the perovskite semiconductor CsPbBr3: a new material for high-energy radiation detection. *Crystal growth & design, 13*(7), 2722-2727.

Tan, Z.-K., Moghaddam, R. S., Lai, M. L., Docampo, P., Higler, R., Deschler, F., . . . Credgington, D. (2014). Bright light-emitting diodes based on organometal halide perovskite. *Nature nanotechnology, 9*(9), 687.

Trots, D., & Myagkota, S. (2008). High-temperature structural evolution of caesium and rubidium triiodoplumbates. *Journal of Physics and Chemistry of Solids, 69*(10), 2520-2526.

Wei, H., Fang, Y., Mulligan, P., Chuirazzi, W., Fang, H.-H., Wang, C., . . . Cao, L. (2016). Sensitive X-ray detectors made of methylammonium lead tribromide perovskite single crystals. *Nature Photonics, 10*(5), 333.

Ye, Y., Run, X., Hai-Tao, X., Feng, H., Fei, X., & Lin-Jun, W. (2015). Nature of the band gap of halide perovskites ABX3 (A= CH3NH3, Cs; B= Sn, Pb; X= Cl, Br, I): First-principles calculations. *Chinese Physics B, 24*(11), 116302.

Zhang, L., Zeng, Q., & Wang, K. (2017). Pressure-induced structural and optical properties of inorganic halide perovskite CsPbBr3. *The journal of physical chemistry letters, 8*(16), 3752-3758.

Zhou, H., Chen, Q., Li, G., Luo, S., Song, T.-b., Duan, H.-S., . . . Yang, Y. (2014). Interface engineering of highly efficient perovskite solar cells. *Science, 345*(6196), 542-546.